

Measurement of the energy dependence of hadronic jet rates and the strong coupling α_s from the four-jet rate with the DELPHI detector at LEP

DELPHI Collaboration

Abstract

Hadronic events from the data collected with the DELPHI detector at LEP within the energy range from 89 GeV to 209 GeV are selected, their jet rates are determined and compared to predictions of four different event generators. One of them is the recently developed APACIC++ generator which performs a massive matrix element calculation matched to a parton shower followed by string fragmentation. The four-jet rate is used to measure α_s in the next-to-leading-order approximation yielding

$$\alpha_s(M_Z^2) = 0.1175 \pm 0.0030.$$

The running of α_s determined by using four-jet events has been tested. The logarithmic energy slope is measured to be

$$\frac{d\alpha_s^{-1}}{d \log E_{\text{cm}}} = 1.14 \pm 0.36.$$

Since the analysis is based on four-jet final states it represents an alternative approach to previous DELPHI α_s measurements using event shape distributions.

J.Abdallah²⁵, P.Abreu²², W.Adam⁵¹, P.Adzic¹¹, T.Albrecht¹⁷, T.Alderweireld², R.Aleman-Fernandez⁸, T.Allmendinger¹⁷, P.P.Allport²³, U.Amaldi²⁹, N.Amapane⁴⁵, S.Amato⁴⁸, E.Anashkin³⁶, A.Andreazza²⁸, S.Andringa²², N.Anjos²², P.Antilogus²⁵, W-D.Apel¹⁷, Y.Arnoud¹⁴, S.Ask²⁶, B.Asman⁴⁴, J.E.Augustin²⁵, A.Augustinus⁸, P.Baillon⁸, A.Ballestrero⁴⁶, P.Bambade²⁰, R.Barbier²⁷, D.Bardin¹⁶, G.Barker¹⁷, A.Baroncelli³⁹, M.Battaglia⁸, M.Baillier²⁵, K-H.Becks⁵³, M.Begalli⁶, A.Behrmann⁵³, E.Ben-Haim²⁰, N.Benekos³², A.Benvenuti⁵, C.Berat¹⁴, M.Berggren²⁵, L.Berntzon⁴⁴, D.Bertrand², M.Besancon⁴⁰, N.Besson⁴⁰, D.Bloch⁹, M.Blom³¹, M.Bluj⁵², M.Bonesini²⁹, M.Boonekamp⁴⁰, P.S.L.Booth²³, G.Borisov²¹, O.Botner⁴⁹, B.Bouquet²⁰, T.J.V.Bowcock²³, I.Boyko¹⁶, M.Bracko⁴³, R.Brenner⁴⁹, E.Brodet³⁵, P.Bruckman¹⁸, J.M.Brunet⁷, L.Bugge³³, P.Buschmann⁵³, M.Calvi²⁹, T.Camporesi⁸, V.Canale³⁸, F.Carena⁸, N.Castro²², F.Cavallo⁵, M.Chapkin⁴², Ph.Charpentier⁸, P.Checchia³⁶, R.Chierici⁸, P.Chliapnikov⁴², J.Chudoba⁸, S.U.Chung⁸, K.Cieslik¹⁸, P.Collins⁸, R.Contri¹³, G.Cosme²⁰, F.Cossutti⁴⁷, M.J.Costa⁵⁰, D.Crennell³⁷, J.Cuevas³⁴, J.D'Hondt², J.Dalmau⁴⁴, T.da Silva⁴⁸, W.Da Silva²⁵, G.Della Ricca⁴⁷, A.De Angelis⁴⁷, W.De Boer¹⁷, C.De Clercq², B.De Lotto⁴⁷, N.De Maria⁴⁵, A.De Min³⁶, L.de Paula⁴⁸, L.Di Ciaccio³⁸, A.Di Simone³⁹, K.Doroba⁵², J.Drees^{53,8}, M.Dris³², G.Eigen⁴, T.Ekelof⁴⁹, M.Ellert⁴⁹, M.Elsing⁸, M.C.Espirito Santo²², G.Fanourakis¹¹, D.Fassouliotis^{11,3}, M.Feindt¹⁷, J.Fernandez⁴¹, A.Ferrer⁵⁰, F.Ferro¹³, U.Flagmeyer⁵³, H.Foeth⁸, E.Fokitis³², F.Fulda-Quenzen²⁰, J.Fuster⁵⁰, M.Gandelman⁴⁸, C.Garcia⁵⁰, Ph.Gavillet⁸, E.Gazis³², R.Gokiel^{8,52}, B.Golob⁴³, G.Gomez-Ceballos⁴¹, P.Goncalves²², E.Graziani³⁹, G.Grosdidier²⁰, K.Grzelak⁵², J.Guy³⁷, C.Haag¹⁷, A.Hallgren⁴⁹, K.Hamacher⁵³, K.Hamilton³⁵, S.Haug³³, F.Hauler¹⁷, V.Hedberg²⁶, M.Hennecke¹⁷, H.Herr⁸, J.Hoffman⁵², S-O.Holmgren⁴⁴, P.J.Holt⁸, M.A.Houlden²³, K.Hultqvist⁴⁴, J.N.Jackson²³, G.Jarlskog²⁶, P.Jarry⁴⁰, D.Jeans³⁵, E.K.Johansson⁴⁴, P.D.Johansson⁴⁴, P.Jonsson²⁷, C.Joram⁸, L.Jungermann¹⁷, F.Kapusta²⁵, S.Katsanevas²⁷, E.Katsoufis³², G.Kernel⁴³, B.P.Kersevan^{8,43}, U.Kerzel¹⁷, A.Kiiskinen¹⁵, B.T.King²³, N.J.Kjaer⁸, P.Kluit³¹, P.Kokkinias¹¹, C.Kourkoulis³, O.Kouznetsov¹⁶, Z.Krumstein¹⁶, M.Kucharczyk¹⁸, J.Lamsa¹, G.Leder⁵¹, F.Ledroit¹⁴, L.Leinonen⁴⁴, R.Leitner³⁰, J.Lemonne², V.Lepeltier²⁰, T.Lesiak¹⁸, W.Liebig⁵³, D.Liko⁵¹, A.Lipniacka⁴⁴, J.H.Lopes⁴⁸, J.M.Lopez³⁴, D.Loukas¹¹, P.Lutz⁴⁰, L.Lyons³⁵, J.MacNaughton⁵¹, A.Malek⁵³, S.Maltesos³², F.Mandl⁵¹, J.Marco⁴¹, R.Marco⁴¹, B.Marechal⁴⁸, M.Margoni³⁶, J-C.Marin⁸, C.Mariotti⁸, A.Markou¹¹, C.Martinez-Rivero⁴¹, J.Masik¹², N.Mastroiannopoulos¹¹, F.Matorras⁴¹, C.Matteuzzi²⁹, F.Mazzucato³⁶, M.Mazzucato³⁶, R.Mc Nulty²³, C.Meroni²⁸, E.Migliore⁴⁵, W.Mitaroff⁵¹, U.Mjoernmark²⁶, T.Moa⁴⁴, M.Moch¹⁷, K.Moenig^{8,10}, R.Monge¹³, J.Montenegro³¹, D.Moraes⁴⁸, S.Moreno²², P.Morettini¹³, U.Mueller⁵³, K.Muenich⁵³, M.Mulders³¹, L.Mundim⁶, W.Murray³⁷, B.Muryn¹⁹, G.Myatt³⁵, T.Myklebust³³, M.Nassiakou¹¹, F.Navarria⁵, K.Nawrocki⁵², R.Nicolaidou⁴⁰, M.Nikolenko^{16,9}, A.Oblakowska-Mucha¹⁹, V.Obratzov⁴², A.Olshevski¹⁶, A.Onofre²², R.Orava¹⁵, K.Osterberg¹⁵, A.Ouraou⁴⁰, A.Oyanguren⁵⁰, M.Paganoni²⁹, S.Paiano⁵, J.P.Palacios²³, H.Palka¹⁸, Th.D.Papadopoulou³², L.Pape⁸, C.Parkes²⁴, F.Parodi¹³, U.Parzefall⁸, A.Passeri³⁹, O.Passon⁵³, L.Peralta²², V.Perepelitsa⁵⁰, A.Perrotta⁵, A.Petrolini¹³, J.Piedra⁴¹, L.Pieri³⁹, F.Pierre⁴⁰, M.Pimenta²², E.Piotto⁸, T.Podobnik⁴³, V.Poireau⁸, M.E.Pol⁶, G.Polok¹⁸, P.Poropat⁴⁷, V.Pozdniakov¹⁶, N.Pukhaeva^{2,16}, A.Pullia²⁹, J.Rames¹², L.Ramler¹⁷, A.Read³³, P.Rebecchi⁸, J.Rehn¹⁷, D.Reid³¹, R.Reinhardt⁵³, P.Renton³⁵, F.Richard²⁰, J.Ridky¹², M.Rivero⁴¹, D.Rodriguez⁴¹, A.Romero⁴⁵, P.Ronchese³⁶, P.Roudeau²⁰, T.Rovelli⁵, V.Ruhlmann-Kleider⁴⁰, D.Ryabtchikov⁴², A.Sadovsky¹⁶, L.Salmi¹⁵, J.Salt⁵⁰, A.Savoy-Navarro²⁵, U.Schwickerath⁸, A.Segar³⁵, R.Sekulin³⁷, M.Siebel⁵³, A.Sisakian¹⁶, G.Smadja²⁷, O.Smirnova²⁶, A.Sokolov⁴², A.Sopczak²¹, R.Sosnowski⁵², T.Spaso⁸, M.Stanitzki¹⁷, A.Stocchi²⁰, J.Strauss⁵¹, B.Stugu⁴, M.Szczekowski⁵², M.Szeptycka⁵², T.Szumlak¹⁹, T.Tabarelli²⁹, A.C.Taffard²³, F.Tegenfeldt⁴⁹, J.Timmermans³¹, L.Tkatchev¹⁶, M.Tobin²³, S.Todorovova¹², B.Tome²², A.Tonazzo²⁹, P.Tortosa⁵⁰, P.Travnicek¹², D.Treille⁸, G.Tristram⁷, M.Trochimczuk⁵², C.Troncon²⁸, M-L.Turluer⁴⁰, I.A.Tyapkin¹⁶, P.Tyapkin¹⁶, S.Tzamarias¹¹, V.Uvarov⁴², G.Valenti⁵, P.Van Dam³¹, J.Van Eldik⁸, A.Van Lysebetten², N.van Remortel², I.Van Vulpen⁸, G.Vegni²⁸, F.Veloso²², W.Venus³⁷, P.Verdier²⁷, V.Verzi³⁸, D.Vilanova⁴⁰, L.Vitale⁴⁷, V.Vrba¹²,

H.Wahlen⁵³, A.J.Washbrook²³, C.Weiser¹⁷, D.Wicke⁸, J.Wickens², G.Wilkinson³⁵, M.Winter⁹, M.Witek¹⁸, O.Yushchenko⁴², A.Zalewska¹⁸, P.Zalewski⁵², D.Zavrtnik⁴³, V.Zhuravlov¹⁶, N.I.Zimin¹⁶, A.Zintchenko¹⁶, M.Zupan¹¹

-
- ¹Department of Physics and Astronomy, Iowa State University, Ames IA 50011-3160, USA
²Physics Department, Universiteit Antwerpen, Universiteitsplein 1, B-2610 Antwerpen, Belgium
and IIHE, ULB-VUB, Pleinlaan 2, B-1050 Brussels, Belgium
and Faculté des Sciences, Univ. de l'Etat Mons, Av. Maistriau 19, B-7000 Mons, Belgium
³Physics Laboratory, University of Athens, Solonos Str. 104, GR-10680 Athens, Greece
⁴Department of Physics, University of Bergen, Allégaten 55, NO-5007 Bergen, Norway
⁵Dipartimento di Fisica, Università di Bologna and INFN, Via Irnerio 46, IT-40126 Bologna, Italy
⁶Centro Brasileiro de Pesquisas Físicas, rua Xavier Sigaud 150, BR-22290 Rio de Janeiro, Brazil
and Depto. de Física, Pont. Univ. Católica, C.P. 38071 BR-22453 Rio de Janeiro, Brazil
and Inst. de Física, Univ. Estadual do Rio de Janeiro, rua São Francisco Xavier 524, Rio de Janeiro, Brazil
⁷Collège de France, Lab. de Physique Corpusculaire, IN2P3-CNRS, FR-75231 Paris Cedex 05, France
⁸CERN, CH-1211 Geneva 23, Switzerland
⁹Institut de Recherches Subatomiques, IN2P3 - CNRS/ULP - BP20, FR-67037 Strasbourg Cedex, France
¹⁰Now at DESY-Zeuthen, Platanenallee 6, D-15735 Zeuthen, Germany
¹¹Institute of Nuclear Physics, N.C.S.R. Demokritos, P.O. Box 60228, GR-15310 Athens, Greece
¹²FZU, Inst. of Phys. of the C.A.S. High Energy Physics Division, Na Slovance 2, CZ-180 40, Praha 8, Czech Republic
¹³Dipartimento di Fisica, Università di Genova and INFN, Via Dodecaneso 33, IT-16146 Genova, Italy
¹⁴Institut des Sciences Nucléaires, IN2P3-CNRS, Université de Grenoble 1, FR-38026 Grenoble Cedex, France
¹⁵Helsinki Institute of Physics, P.O. Box 64, FIN-00014 University of Helsinki, Finland
¹⁶Joint Institute for Nuclear Research, Dubna, Head Post Office, P.O. Box 79, RU-101 000 Moscow, Russian Federation
¹⁷Institut für Experimentelle Kernphysik, Universität Karlsruhe, Postfach 6980, DE-76128 Karlsruhe, Germany
¹⁸Institute of Nuclear Physics, Ul. Kawiora 26a, PL-30055 Krakow, Poland
¹⁹Faculty of Physics and Nuclear Techniques, University of Mining and Metallurgy, PL-30055 Krakow, Poland
²⁰Université de Paris-Sud, Lab. de l'Accélérateur Linéaire, IN2P3-CNRS, Bât. 200, FR-91405 Orsay Cedex, France
²¹School of Physics and Chemistry, University of Lancaster, Lancaster LA1 4YB, UK
²²LIP, IST, FCUL - Av. Elias Garcia, 14-1º, PT-1000 Lisboa Codex, Portugal
²³Department of Physics, University of Liverpool, P.O. Box 147, Liverpool L69 3BX, UK
²⁴Dept. of Physics and Astronomy, Kelvin Building, University of Glasgow, Glasgow G12 8QQ
²⁵LPNHE, IN2P3-CNRS, Univ. Paris VI et VII, Tour 33 (RdC), 4 place Jussieu, FR-75252 Paris Cedex 05, France
²⁶Department of Physics, University of Lund, Sölvegatan 14, SE-223 63 Lund, Sweden
²⁷Université Claude Bernard de Lyon, IPNL, IN2P3-CNRS, FR-69622 Villeurbanne Cedex, France
²⁸Dipartimento di Fisica, Università di Milano and INFN-MILANO, Via Celoria 16, IT-20133 Milan, Italy
²⁹Dipartimento di Fisica, Univ. di Milano-Bicocca and INFN-MILANO, Piazza della Scienza 2, IT-20126 Milan, Italy
³⁰IPNP of MFF, Charles Univ., Areal MFF, V Holesovickach 2, CZ-180 00, Praha 8, Czech Republic
³¹NIKHEF, Postbus 41882, NL-1009 DB Amsterdam, The Netherlands
³²National Technical University, Physics Department, Zografou Campus, GR-15773 Athens, Greece
³³Physics Department, University of Oslo, Blindern, NO-0316 Oslo, Norway
³⁴Dpto. Física, Univ. Oviedo, Avda. Calvo Sotelo s/n, ES-33007 Oviedo, Spain
³⁵Department of Physics, University of Oxford, Keble Road, Oxford OX1 3RH, UK
³⁶Dipartimento di Fisica, Università di Padova and INFN, Via Marzolo 8, IT-35131 Padua, Italy
³⁷Rutherford Appleton Laboratory, Chilton, Didcot OX11 0QX, UK
³⁸Dipartimento di Fisica, Università di Roma II and INFN, Tor Vergata, IT-00173 Rome, Italy
³⁹Dipartimento di Fisica, Università di Roma III and INFN, Via della Vasca Navale 84, IT-00146 Rome, Italy
⁴⁰DAPNIA/Service de Physique des Particules, CEA-Saclay, FR-91191 Gif-sur-Yvette Cedex, France
⁴¹Instituto de Física de Cantabria (CSIC-UC), Avda. los Castros s/n, ES-39006 Santander, Spain
⁴²Inst. for High Energy Physics, Serpukov P.O. Box 35, Protvino, (Moscow Region), Russian Federation
⁴³J. Stefan Institute, Jamova 39, SI-1000 Ljubljana, Slovenia and Laboratory for Astroparticle Physics,
Nova Gorica Polytechnic, Kostanjevska 16a, SI-5000 Nova Gorica, Slovenia,
and Department of Physics, University of Ljubljana, SI-1000 Ljubljana, Slovenia
⁴⁴Fysikum, Stockholm University, Box 6730, SE-113 85 Stockholm, Sweden
⁴⁵Dipartimento di Fisica Sperimentale, Università di Torino and INFN, Via P. Giuria 1, IT-10125 Turin, Italy
⁴⁶INFN, Sezione di Torino, and Dipartimento di Fisica Teorica, Università di Torino, Via P. Giuria 1,
IT-10125 Turin, Italy
⁴⁷Dipartimento di Fisica, Università di Trieste and INFN, Via A. Valerio 2, IT-34127 Trieste, Italy
and Istituto di Fisica, Università di Udine, IT-33100 Udine, Italy
⁴⁸Univ. Federal do Rio de Janeiro, C.P. 68528 Cidade Univ., Ilha do Fundão BR-21945-970 Rio de Janeiro, Brazil
⁴⁹Department of Radiation Sciences, University of Uppsala, P.O. Box 535, SE-751 21 Uppsala, Sweden
⁵⁰IFIC, Valencia-CSIC, and D.F.A.M.N., U. de Valencia, Avda. Dr. Moliner 50, ES-46100 Burjassot (Valencia), Spain
⁵¹Institut für Hochenergiephysik, Österr. Akad. d. Wissensch., Nikolsdorfergasse 18, AT-1050 Vienna, Austria
⁵²Inst. Nuclear Studies and University of Warsaw, Ul. Hoza 69, PL-00681 Warsaw, Poland
⁵³Fachbereich Physik, University of Wuppertal, Postfach 100 127, DE-42097 Wuppertal, Germany

1 Introduction

Measurements of hadronic multijet rates in electron-positron annihilation provide an excellent test of perturbative quantum chromodynamics (QCD). They can be confronted with predictions of QCD-based hadronisation models and allow a precise determination of the strong coupling α_s . Furthermore, the study of multijet production originating from QCD processes is essential for the understanding of the background to four-quark production in W^+W^- or ZZ decays and also for understanding the background in the search for new phenomena. Here we report the final measurements of 2-, 3-, 4-, and 5-jet rates using all data collected by DELPHI during the years 1993 to 2000. The 4-jet rate is used to determine α_s .

Until 1995 the large electron-positron storage ring LEP at CERN operated at centre-of-mass energies around the Z resonance. Due to the high cross-section the total number of hadronic events collected during this part of the LEP1 phase is about 2.5 million. Analysing LEP1 data enables precise measurements of the strong coupling and detailed comparisons of different methods for extracting α_s , see e.g. [1]. From autumn 1995 onwards the centre-of-mass energy was continuously increased and finally reached about 209 GeV in October 2000. During the LEP2 programme DELPHI collected a total of about 12000 hadronic $q\bar{q}$ events at centre-of-mass energies between 130 GeV and 209 GeV. The statistics of hadronic events collected at LEP2, though small compared to that gathered near the Z resonance, are sufficient for the measurement of jet rates and for a determination of the strong coupling α_s , see e.g. [2]. Analysing both LEP1 and LEP2 data gives access to the energy dependence, the running of the strong coupling and thus to a direct test of asymptotic freedom.

In Sec. 2 the selection of hadronic events, the reconstruction of the centre-of-mass energy, the correction procedures applied to the data and the suppression of W^+W^- and ZZ events (and other four-fermion background) are briefly discussed. Sec. 3 presents the applied jet clustering algorithms, the measured jet rates and the comparison of the data with predictions from hadronic event generators. In Sec. 4, the measurement of α_s based on the 4-jet data is presented. As in all analyses using topological information from hadronic events, the error on the value of α_s is dominated by theoretical uncertainties. Here we determine α_s by applying second order perturbation theory with an optimised renormalisation scale. In Sec. 4, the α_s measurements along with studies of different choices of the renormalisation scale and the investigation of the running of α_s from LEP1 and LEP2 data are presented.

2 Selection and correction of hadronic data

The analysis uses data taken with the DELPHI detector at centre-of-mass energies between 89 GeV and 209 GeV divided into 14 energy bins. Data entering the analysis, including the integrated luminosities collected at these energies and the cross-sections of the contributing processes, are summarised in Table 1.

DELPHI is a hermetic detector with a solenoidal magnetic field of 1.2T. The tracking detectors in the barrel part (starting from the beam pipe) are a silicon micro-vertex detector (VD), a combined jet/proportional chamber inner detector (ID), a time projection chamber (TPC) as the main tracking device, and a streamer tube detector (OD) in the barrel region. The forward region is covered by silicon mini-strip and pixel detectors (VFT) and by the drift chamber detectors (FCA and FCB).

	E_{cm} [GeV]	year	\mathcal{L} [pb^{-1}]	$\sigma_{q\bar{q}}$ [pb]	$\sigma_{q\bar{q}}^{\sqrt{s_{\text{rec}}^I > 0.9 \cdot \sqrt{s}}}$ [pb]	σ_{WW} [pb]	σ_{ZZ} [pb]	$N_{\text{had.}}$
LEP1	89.4	1993/95	18.6	9900.	—	—	—	163 013
	91.2	1993/94/95	77.4	30 400.	—	—	—	2 091 448
	93.0	1993/95	13.8	14100.	—	—	—	237 674
LEP2	133.2	1995	11.9	292.0	69.2	—	—	846
		1997						
	161.4	1996	11.5	147.0	32.3	3.4	—	358
	172.3		10.8	121.0	27.5	12.3	—	261
	183.1	1997	57.9	100.3	23.4	16.5	1.0	1 173
	189.2	1998	157.0	99.8	21.1	17.5	1.6	3 053
	192.2	1999	25.2	96.0	20.2	18.1	1.7	466
	196.2		78.4	90.0	19.2	18.6	1.7	1 338
	200.1		81.8	85.2	18.2	18.7	1.8	1 339
	202.1		39.8	83.3	17.7	18.8	1.8	642
	204.9	2000	76.1	80.0	17.0	18.9	1.8	1 187
206.8	84.1		77.7	16.5	18.9	1.8	1 297	

Table 1: *Data entering the analysis: the columns show the mean centre-of-mass energies E_{cm} , the years of data taking, the integrated luminosities, the cross-sections for $q\bar{q}$ (before and after the cut on the effective centre-of-mass energy $\sqrt{s_{\text{rec}}^I} > 0.9 \cdot E_{\text{cm}}$, described in the text), W^+W^- , and neutral boson pair production (from Zfitter6.21 [3]) and the number of selected $q\bar{q}$ events after the cuts described in the text.*

Track selection	$0.4 \text{ GeV} \leq p \leq 100 \text{ GeV}$ $\Delta p/p \leq 1.0$ measured track length $\geq 30 \text{ cm}$ distance to I.P. in $r\phi$ plane $\leq 4 \text{ cm}$ distance to I.P. in $z \leq 10 \text{ cm}$
Event selection	$N_{\text{charged}} \geq 7$ $25^\circ \leq \theta_{\text{thrust}} \leq 155^\circ$
ISR cuts	$E_{\text{tot}} \geq 0.50 \cdot E_{\text{cm}}$ $\sqrt{s'_{\text{rec}}} \geq 0.9 \cdot E_{\text{cm}}$
WW and 4f cuts	$D^2 > 900 \text{ GeV}^2$ $42 \geq N_{\text{charged}}$

Table 2: Criteria for track- and event selection. p is the momentum, Δp its error, r the radial distance to the beam-axis, z the distance to the beam interaction point (I.P.) along the beam-axis, ϕ the azimuthal angle, N_{charged} the number of charged particles, θ_{thrust} the polar angle of the thrust axis with respect to the beam, E_{tot} the total energy carried by all measured particles, $\sqrt{s'_{\text{rec}}}$ the effective centre-of-mass energy, $E_{\text{cm}} = 2E_{\text{beam}} = \sqrt{s}$ the nominal centre-of-mass energy, and D^2 the discrimination variable, defined in Eq. 1. The first two cuts apply to charged and neutral particles, while the other track selection cuts apply only to charged particles.

The electromagnetic calorimeters are the high density projection chamber (HPC) in the barrel, and the lead-glass calorimeter (FEMC) in the forward region. The hadron calorimeter (HCAL) is a sampling gas detector incorporated in the magnet yoke. Detailed information about the design and performance of DELPHI can be found in [4, 5].

In order to select well measured charged particle tracks, the cuts given in the upper part of Table 2 have been applied. The cuts in the lower part of the table are used to select $e^+e^- \rightarrow Z/\gamma \rightarrow q\bar{q}$ events and to suppress background processes such as two-photon interactions, beam-gas and beam-wall interactions, leptonic final states, and, for the LEP2 analysis, initial state radiation (ISR) and four-fermion (4f) background.

At energies above 91.2 GeV, the large cross-section of the Z resonance peak raises the possibility of hard initial state radiation (ISR) allowing the creation of a nearly on-shell Z boson. These “radiative return events” constitute a large fraction of all hadronic events. The ISR photons are typically aligned along the beam direction and usually escape detection. In order to evaluate the effective hadronic centre-of-mass energy $\sqrt{s'}$ of an event, considering ISR, an algorithm called SPRIME is used [6]. SPRIME is based on a fit imposing four-momentum conservation to measured jet four-momenta (including estimates of their errors). The hypotheses of single and multi photon radiation are tested based on the χ^2 obtained in the corresponding constrained fits.

Figure 1 shows the 189 and 200 GeV effective centre-of-mass energy spectra as computed with SPRIME for simulated and measured events passing all but the $\sqrt{s'_{\text{rec}}}$ cut. A cut on the reconstructed centre-of-mass energy $\sqrt{s'_{\text{rec}}} \geq 0.9 \cdot E_{\text{cm}}$ is applied to discard radiative return events (see Table 2). Two-photon events, leptonic events and events due to leptonic or semileptonic W^+W^- decays are strongly suppressed by the cuts. The re-

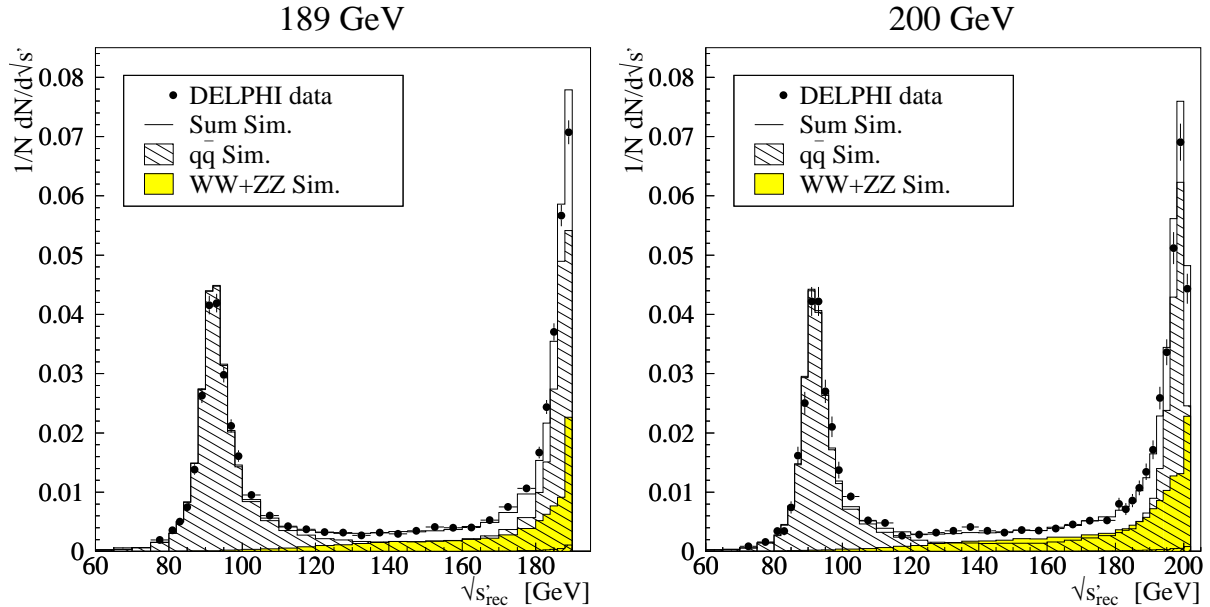


Figure 1: *Reconstructed centre of mass energy $\sqrt{s'_{\text{rec}}}$ before all cuts except the one on $\sqrt{s'_{\text{rec}}}$ compared to QCD and four-fermion simulations. The small differently shaded areas in the bottom right of the plots indicate the size of WW and neutral boson pair background.*

maining background from these types of events was found to be negligible in the following analysis.

Since the topological signatures of QCD four-jet events and hadronic 4f events are similar, no highly efficient separation of the two classes of events is possible. Furthermore any 4f rejection implies a bias to the shape distributions of QCD events, which needs to be corrected with simulation. In this analysis a cut in the discrimination variable D^2 [7] is applied to separate four-jet QCD events from hadronic W^+W^- decays. All events are forced into a four-jet configuration by a clustering algorithm. From the resulting four-momenta of the pseudo-particles the following quantity is calculated:

$$D^2 = \min \{ (M_{ij} - M_W)^2 + (M_{kl} - M_W)^2 \} \quad (1)$$

$$(ij; kl) = (12; 34), (13; 24), (14; 23).$$

The discrimination variable D^2 is based on a comparison of invariant dijet masses to the nominal mass of the W boson. The minimum difference for all possible jet pairings (ij, kl) is expected to be small for events arising from boson pair production. Figure 2 shows the distribution of D^2 at 205 and 207 GeV, compared to the simulation of contributing processes. Events from W^+W^- or neutral boson pair production cluster at small values of D^2 , while $e^+e^- \rightarrow Z/\gamma \rightarrow q\bar{q}$ events extend to larger values of D^2 . Demanding $D^2 > 900 \text{ GeV}^2$ leads to an efficient suppression of W^+W^- and neutral boson pair events. All remaining 4f contributions are estimated by using Monte Carlo generators and subtracted from the measurement. The simulations are normalised using the cross-sections given in Table 1. The quoted σ_{WW} values correspond to a W mass of 80.35 GeV. For the simulation of WW and ZZ events the following generators were used:

- EXCALIBUR [8] generates four-fermion final states through all possible electroweak four-fermion processes. The generator includes the width of the W and Z bosons.

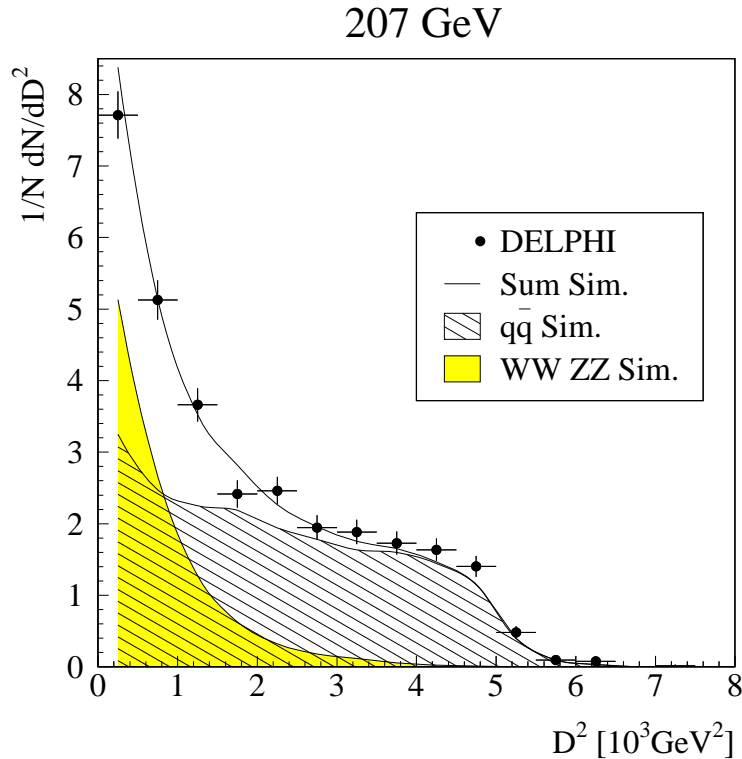


Figure 2: *Distribution of D^2 for accepted data at 207 GeV before applying four-fermion cuts, compared to $q\bar{q}$ and $4f$ simulation.*

QED initial state corrections are implemented using a structure function formalism [9]. EXCALIBUR also includes a Coulomb correction [11] for the CC03 WW production [10].

- PYTHIA 5.7 [12] is a general-purpose Monte Carlo generator for multi-particle production in high energy physics. As a general-purpose generator it does not contain the detailed modelling of all the specific corrections that are contained in the dedicated four-fermion generators.

For the central result the EXCALIBUR generator was applied while the difference between PYTHIA and EXCALIBUR was used to estimate the systematic uncertainty on the background subtraction (see Sec. 4.5).

Detector and cut effects are unfolded with simulation. The influence of detector effects was studied by passing generated events (JETSET/PYTHIA [13] using the DELPHI tuning described in [14]) through a full detector simulation (DELSIM [4]). These Monte Carlo events are processed with the reconstruction program applying selection cuts as for the real data. In order to correct for cuts, detector and ISR effects, a bin-by-bin acceptance correction C , obtained from $e^+e^- \rightarrow Z/\gamma \rightarrow q\bar{q}$ simulation, is applied to the data:

$$C_{det,i} = \frac{h(f_i)_{gen,noISR}}{h(f_i)_{acc}}, \quad (2)$$

where $h(f_i)_{gen,noISR}$ represents bin i of the shape distribution f generated with the tuned generator. The subscript noISR indicates that only events without large ISR ($\sqrt{s} -$

$\sqrt{s'_{\text{rec}}} < 0.1 \text{ GeV}$) enter the distribution. $h(f_i)_{\text{acc}}$ represents the accepted distribution f as obtained with the full detector simulation.

3 Jet rates

Jet clustering algorithms are applied to cluster the large number of particles of a hadronic event into a small number of jets, reflecting the structure of hard partons of the event. Most clustering algorithms in e^+e^- annihilation apply a recursive scheme based on an ordering variable d_{ij} , a distance measure y_{ij} and a merging scheme indicated by \oplus in the following, all being functions of the four-momenta p of two objects i and j . The algorithms start with a table of particles representing the initial objects. The pair of objects with the smallest d_{ij} is considered for merging. These two objects are merged into one new object by applying the merging scheme $p_k = p_i \oplus p_j$, provided that the distance measure y_{ij} is smaller than some given maximum separation y_{cut} . This step is repeated with the two particles i and j replaced by the combined object k . After each iteration the ordering variables d_{ij} have to be recalculated. The iteration stops if only one object remains or if all distance measures y_{ij} are larger than y_{cut} .

The remaining objects are called *jets* and the number of jets n is a function of the cutoff parameter y_{cut} .

The n -jet rate, $R_n(y_{\text{cut}})$ gives the fraction of n -jet events relative to all events. By definition:

$$\sum_i R_i(y_{\text{cut}}) \equiv 1. \quad (3)$$

The details of the clustering algorithms used in this analysis are defined below.

3.1 JADE

The JADE algorithm [15] is based on the same distance measure and ordering variable:

$$d_{ij} = y_{ij} = \frac{2E_i E_j \cdot (1 - \cos \theta_{ij})}{E_{\text{vis}}^2}, \quad (4)$$

E_{vis} being the visible energy, which would be the centre of mass energy E_{cm} for a perfect detector, E_i, E_j being the energy of the objects i and j and θ_{ij} being the angle between \vec{p}_i and \vec{p}_j .

The merging scheme simply adds the four momenta of p_i and p_j :

$$p_k = p_i \oplus p_j = p_i + p_j. \quad (5)$$

There are shortcomings within JADE arising from the choice of the distance measure y_{ij} . For events with soft gluons radiated off the quark and the antiquark, there are kinematical regions where JADE combines the soft gluons first. The resulting ‘‘phantom’’ jet has a resultant momentum at large angle to the initial quarks and may point to a region where no particles exist.

3.2 DURHAM

In case of the DURHAM or k_{\perp} algorithm [16] the distance measure d_{ij} and the ordering variable y_{ij} are the same but they are now changed from mass to normalised transverse

momentum k_{\perp} .

$$d_{ij} = y_{ij} = \frac{2 \cdot \min \{E_i^2, E_j^2\} \cdot (1 - \cos \theta_{ij})}{E_{\text{vis}}^2}. \quad (6)$$

This choice mitigates the shortcomings of the JADE algorithm.

3.3 CAMBRIDGE

The CAMBRIDGE algorithm [17] is a modified k_{\perp} clustering algorithm similar to the DURHAM algorithm. It is designed to preserve the advantages of DURHAM while reducing non-perturbative corrections at small y and providing better resolution of jet substructure. CAMBRIDGE is based on the same distance measure y_{ij} as DURHAM (Eq.5, 6). The ordering variable d_{ij} is a function of the angle between the objects i and j (“angular ordering”):

$$d_{ij} = 2 \cdot (1 - \cos \theta_{ij}) . \quad (7)$$

If $y_{ij} \geq y_{\text{cut}}$ the object with the smaller energy is stored as a jet and deleted from the event table (“soft freezing”). If $y_{ij} < y_{\text{cut}}$ the objects are merged into a new object. The iteration stops if only one object remains or if all distance measures y_{ij} are larger than y_{cut} .

3.4 Results

Figure 3 shows the CAMBRIDGE four-jet rate R_4 as a function of y_{cut} from the 207 GeV data before and after the $D^2 > 900 \text{ GeV}^2$ cut and underlines the separation power of D^2 . The data are found to be in good agreement with the simulation.

The remaining amount of four-fermion background is subtracted to obtain the final data points given in Figures 4, 5 and 6 showing the jet rates R_2 , R_3 , R_4 and R_5 as determined with the JADE, DURHAM and CAMBRIDGE jet algorithms at 91 GeV and for a sample of LEP2 energies. Within errors, the 2-, 3-, and 4-jet rates show a good overall agreement at all energies with the generator predictions tuned to data at the Z resonance. Figures 7 and 8 show a detailed comparison between CAMBRIDGE jet rates and Monte Carlo predictions. Several models, tuned to DELPHI data, are available [14, 18] and are used within this analysis:

- PYTHIA 6.1 is a parton-shower model with explicit angular ordering, followed by string fragmentation [12].
- ARIADNE 4.08 performs a colour-dipole cascade, followed by string fragmentation [19].
- HERWIG 6.1 is a coherent parton-shower model, followed by cluster fragmentation [20].
- APACIC++ performs a massive leading-order (LO) matrix element (ME) calculation for 3-, 4-, and 5-jet final states, matched to a parton-shower and followed by Lund string fragmentation [21–23]. The APACIC++ parameters have been tuned to DELPHI data measured at the Z resonance.

The precise LEP1 data in particular allow a critical judgment of the precision of tuned Monte Carlo models [18]. The parton-shower model PYTHIA tends to overestimate the 3-jet rate and to underestimate the 4-jet rate at large y_{cut} , see also Figure 4. To cure the lack of multijet events a calculation of the underlying matrix elements has been performed. APACIC++ also tends to overestimate the 3-jet rate but predicts more 4-jet events at small y_{cut} . By taking quark mass effects into account the agreement with the

data improves somewhat. The parton-shower generator HERWIG also gives an acceptable agreement with the data. The best overall agreement is obtained with the colour-dipole model ARIADNE. At LEP2 energies the deviations are obscured by the larger statistical errors. Within errors all models show good agreement with the data. Note that the errors shown are statistical only and that neighbouring bins are correlated. Considering the experimental errors and model uncertainties, no significant excess of multijet events at higher energies is observed.

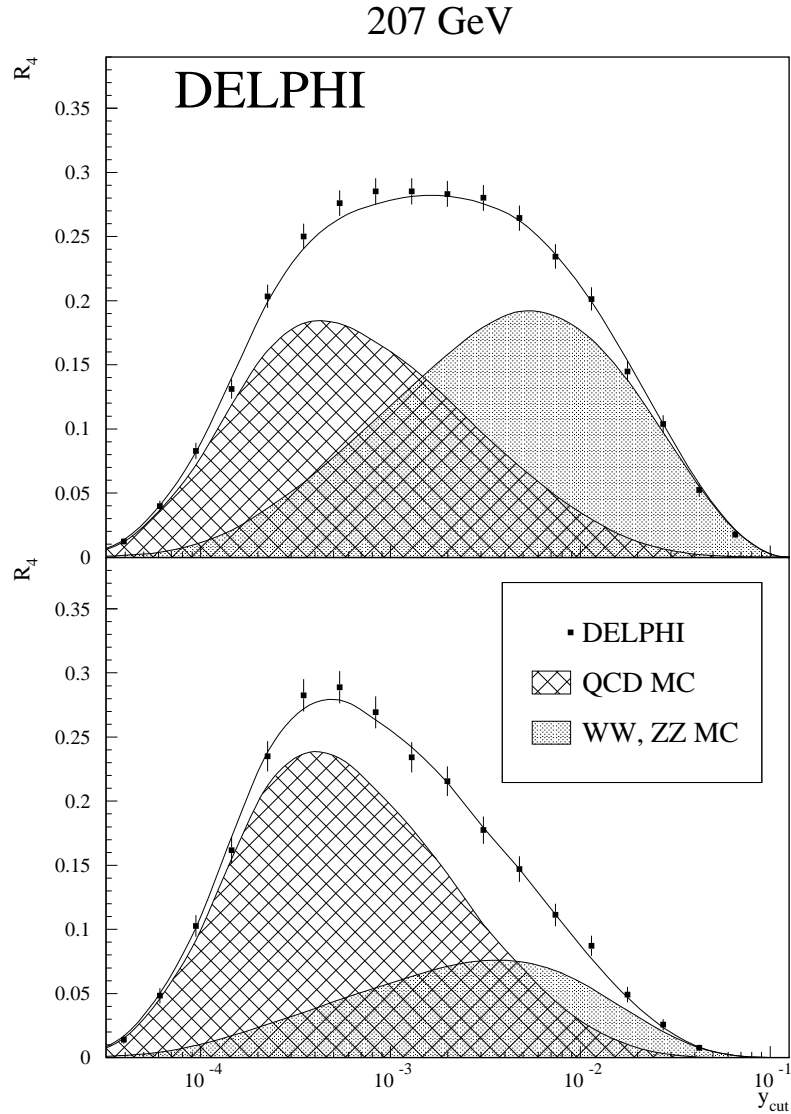


Figure 3: Four-jet rate (R_4), determined with the CAMBRIDGE algorithm, from raw data at 207 GeV as a function of y_{cut} , compared to the simulation of the contributing processes. Top: before cuts against four-fermion background. Bottom: After cutting at $D^2 > 900 \text{ GeV}^2$.

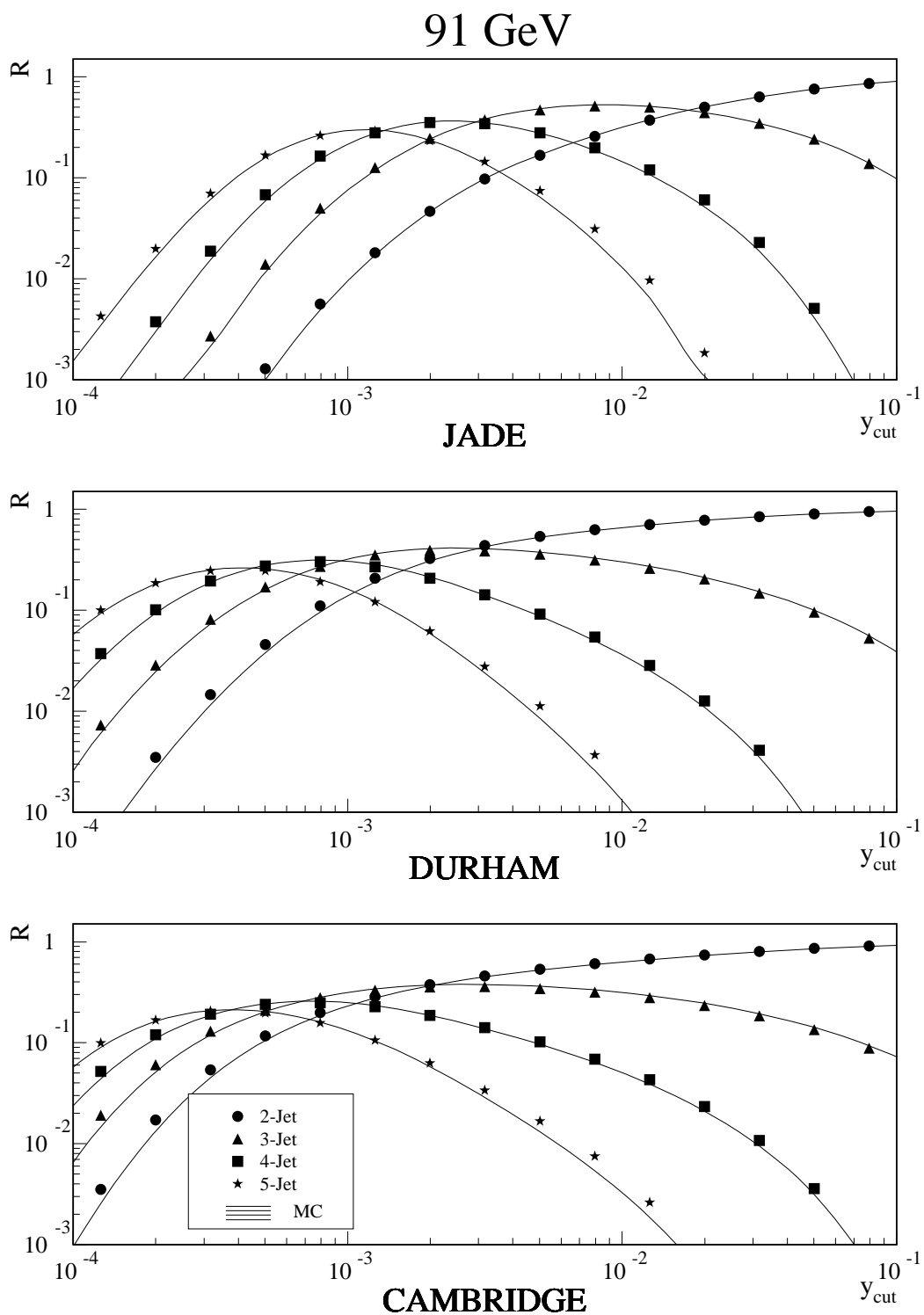


Figure 4: Jet rates (R) at 91 GeV as a function of y_{cut} compared to the prediction of *PYTHIA 6.1*

Figure 5: Jet rates (R) at 133 and 189 GeV as a function of y_{cut} compared to the prediction of PYTHIA 6.1.

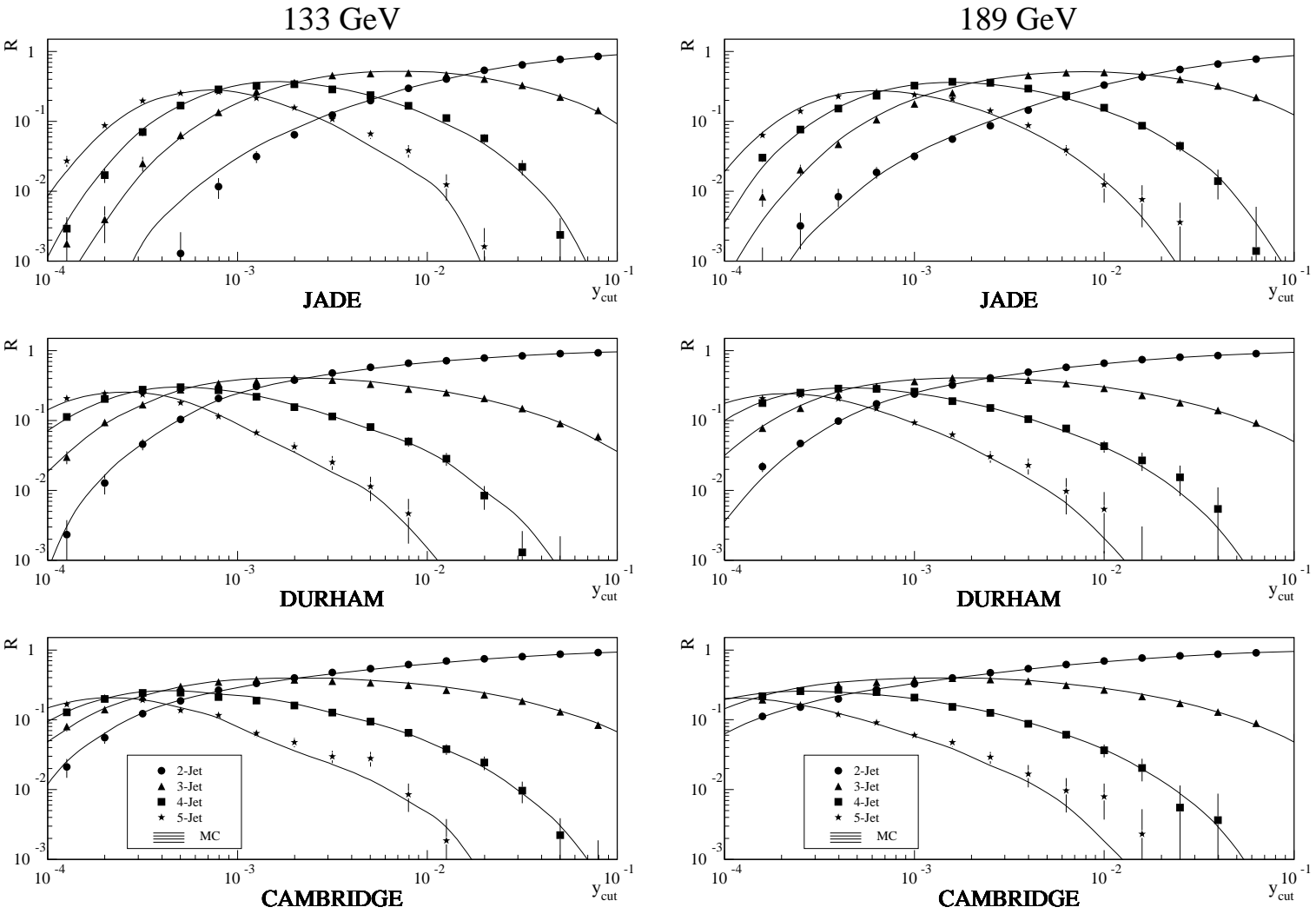
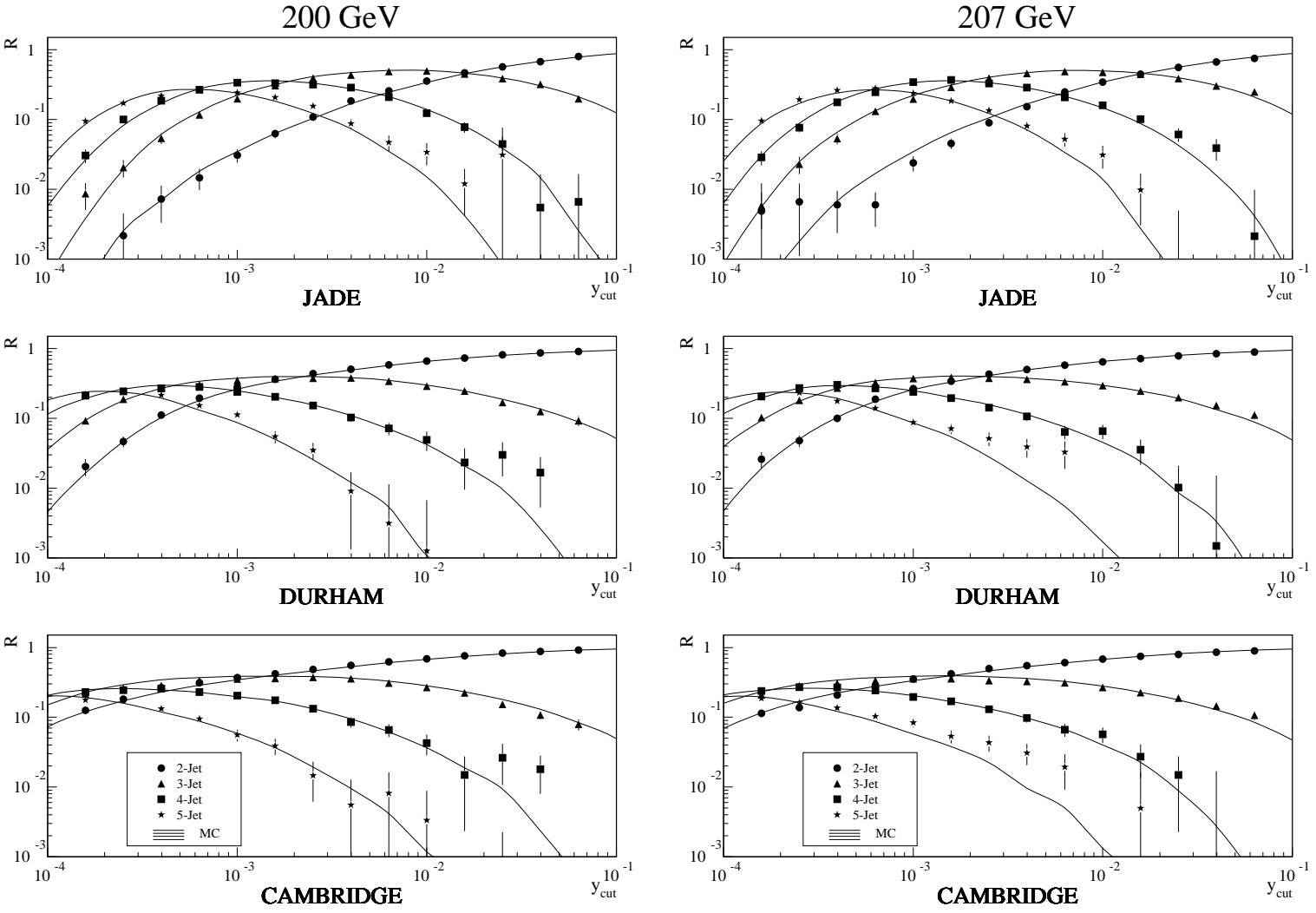


Figure 6: Jet rates (R) at 200 and 207 GeV as a function of y_{cut} compared to the prediction of PYTHIA 6.1.



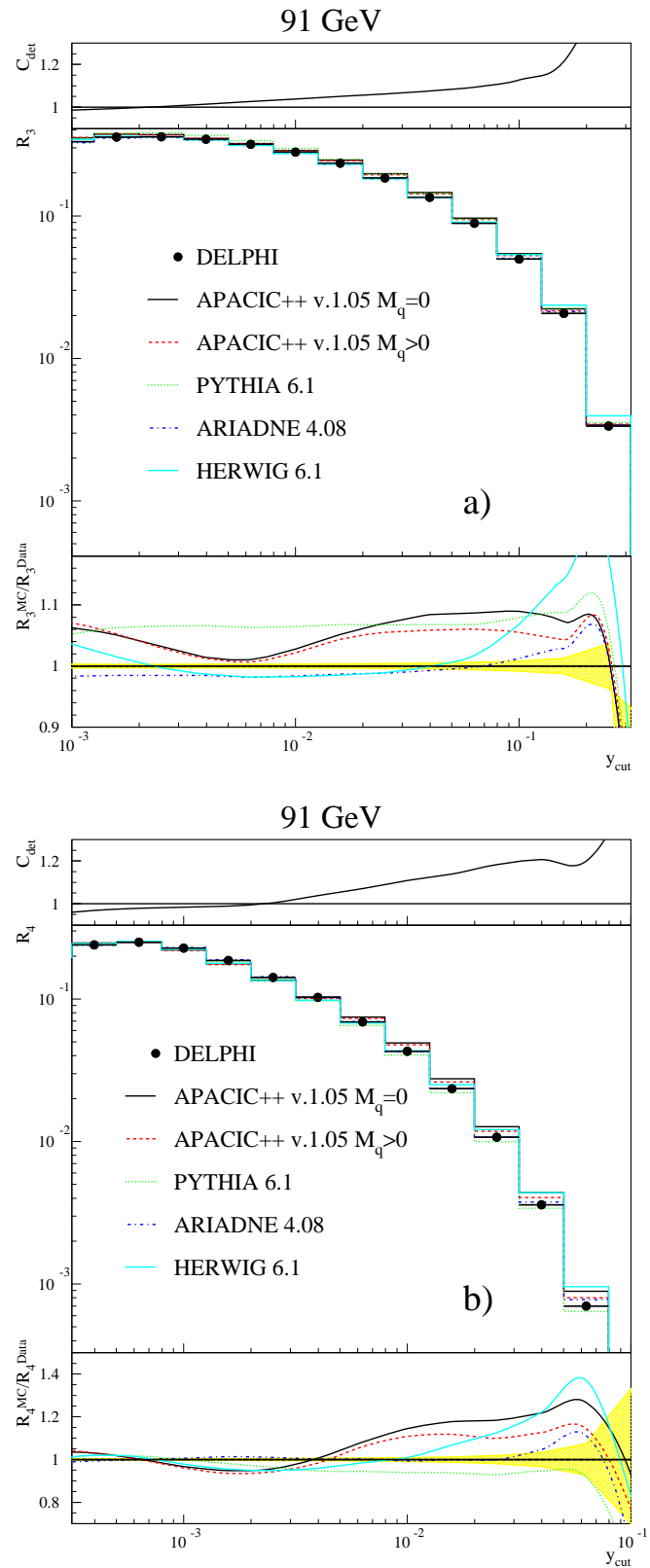


Figure 7: Jet rates determined with the CAMBRIDGE algorithm. a) 3-jet rate at 91 GeV. b) 4-jet rate at 91 GeV. The upper inset shows the corrections C_{det} applied to the data. The central plot shows the jet rates with their statistical error in comparison with different Monte Carlo predictions. The lower inset shows the jet rates normalized to the data. The band indicates the statistical

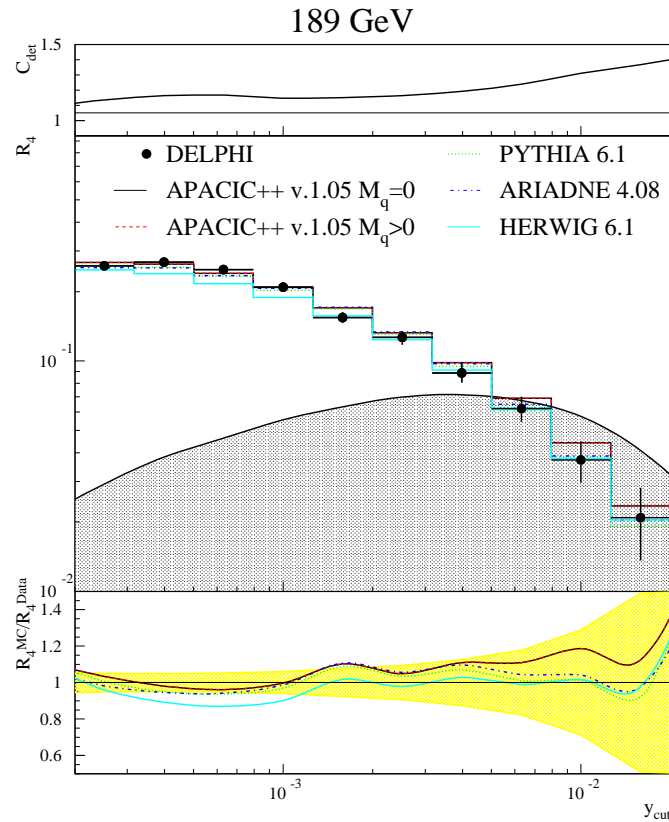


Figure 8: 4-jet rate at 189 GeV determined with the CAMBRIDGE algorithm. The upper inset shows the corrections C_{det} applied to the data. The central plot shows the jet rates with their statistical error in comparison with different Monte Carlo predictions. The grey area in the central plot shows the already subtracted background of WW and ZZ events. The lower inset shows the jet rates normalised to the data. The band indicates the statistical and systematical uncertainty of the data.

4 Determination of α_s

The strong coupling constant, α_s , is determined from the four-jet rate, by fitting an α_s -dependent QCD prediction folded with a hadronisation correction to the data.

4.1 NLO predictions

The next-to-leading-order (NLO) expression of the four-jet rate is given by:

$$R_4(y) = B(y) \cdot \alpha_s^2 + [C(y) + 2B(y) \cdot b_0 \cdot \ln x_\mu] \cdot \alpha_s^3 + \dots \quad (8)$$

Where $x_\mu = \mu^2/Q^2$, μ being the renormalisation scale, Q the centre-of-mass energy of the event, $b_0 = (33 - 2n_f)/12\pi$ and n_f the number of active flavours. Eq. 8 shows the explicit dependence of R_4 on the renormalisation scale μ . The coefficients $B(y)$ and $C(y)$ for the DURHAM and the CAMBRIDGE algorithms are obtained by integrating the massless matrix elements for e^+e^- annihilations into four-parton final states, performed by the NLO generator DEBRECEN [24, 25]. The R_4 results obtained with the JADE algorithm are not used for the α_s determination because of phantom jets and larger hadronisation corrections.

Figure 9 shows the dependence of R_4 on x_μ . For small values of x_μ the overshoot of the NLO expression changes into an underestimate of the observed/measured R_4 . Thus small values of x_μ are expected when fitting the data, suggesting important contributions of higher-order corrections of $\mathcal{O}(\alpha_s^4)$.

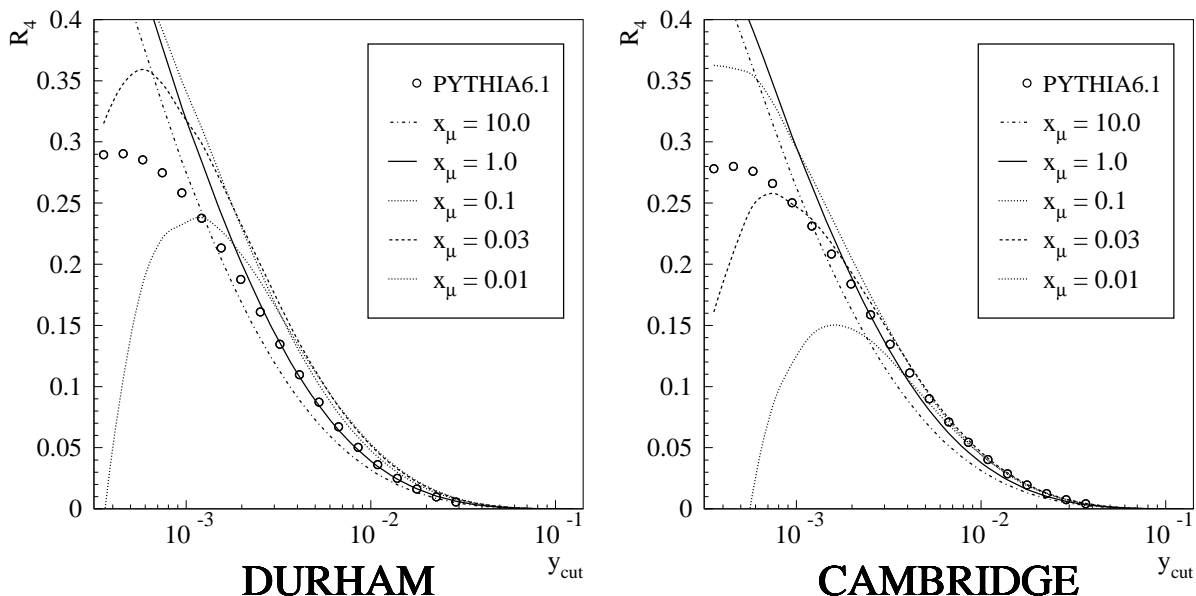


Figure 9: Predictions (left for DURHAM, right for CAMBRIDGE) of the four-jet rate R_4 at 91 GeV using DEBRECEN and Eq. 8 for various values of x_μ at fixed $\alpha_s = 0.118$. Illustrated is the change of the prediction with varying x_μ . The analytical calculations are compared to the parton level prediction using the PYTHIA generator.

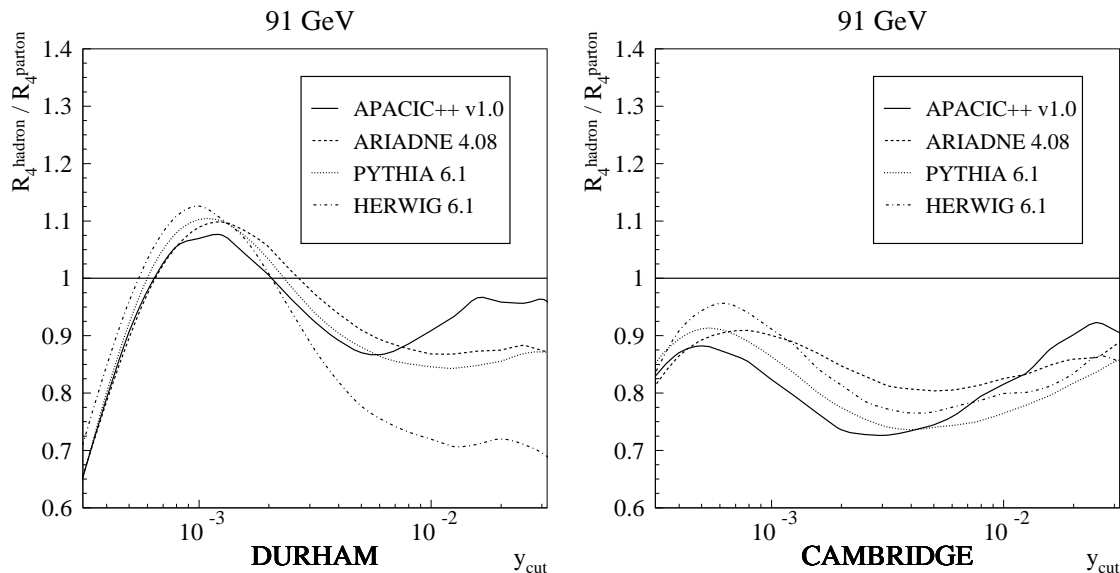


Figure 10: *Distribution of the hadronisation corrections to the four-jet rate. The plots show the ratio of the four-jet rates after and before simulation of the fragmentation, evaluated with different Monte Carlo models.*

4.2 Hadronisation

Before comparing Eq. 8 with the data and fitting its parameters α_s (and x_μ), the transition of coloured partons into colourless hadrons has to be accounted for. This transition has been simulated using Monte Carlo fragmentation models. For each centre-of-mass energy the QCD prediction is multiplied by the hadronisation correction

$$C_{\text{had}}(E_{\text{cm}}) = \frac{f_{\text{had}}^{\text{Sim.}}(E_{\text{cm}})}{f_{\text{part}}^{\text{Sim.}}(E_{\text{cm}})} \quad , \quad (9)$$

where $f_{\text{had}}^{\text{Sim.}}(E_{\text{cm}})$ ($f_{\text{part}}^{\text{Sim.}}(E_{\text{cm}})$) is the model prediction on the hadron (parton) level at the centre-of-mass energy E_{cm} . The parton level is defined as the final state of the parton shower created by the Monte Carlo event generation.

The matching of ME calculations with a parton shower within APACIC++ allows the tuning, performed at LEP1 energies, to be extrapolated. Thus APACIC++ is the only ME generator available at LEP2 energies. Therefore APACIC++ is taken as the reference model. The scatter of results in α_s , when using different Monte Carlo generators is added to the systematic error. Figure 10 shows the ratios between hadron level and parton level as a function of y_{cut} from different generators. Using the CAMBRIDGE algorithm the ratio $R_4^{\text{hadron}}/R_4^{\text{parton}}$ shows a weaker y_{cut} dependence than the same ratio determined by using DURHAM.

4.3 Dependence on the renormalisation scale μ

The explicit dependence of α_s derived from Eq. 8 on the renormalisation scale x_μ arises from the truncation of the perturbative series after a fixed number of orders. Within perturbative QCD x_μ is an arbitrary parameter. A conventional scale setting called “physical scale” is the choice $x_\mu = 1$. However, several other proposals for evaluating the

renormalisation scale are available in the literature. Two of them are investigated within this analysis:

- Method of effective charges (ECH) [26]:

In $\mathcal{O}(\alpha_s^3)$ perturbation theory, the ECH scale value has to be chosen in such a way that the third-order term vanishes:

$$C(y) + 2B(y) \cdot b_0 \cdot \ln x_\mu = 0. \quad (10)$$

- Principle of minimal sensitivity (PMS) [27]:

The PMS optimisation amounts to the determination of the renormalisation scale value, which minimises the sensitivity of the theoretical prediction with respect to its variation:

$$\frac{d}{dx_\mu} [C(y) + 2B(y) \cdot b_0 \cdot \ln x_\mu] = 0. \quad (11)$$

Within both theoretical scale-setting methods the scale x_μ is a function of y_{cut} . The uncertainty of the scale is conventionally estimated by a scale variation within an ad hoc chosen range.

In perturbative QCD the x_μ dependence of the prediction for an observable R would vanish in the all orders limit only. It has been shown in [1] that an excellent description of precise m_Z data can be obtained by fitting simultaneously α_s and x_μ . In the same way a simultaneous fit of α_s and x_μ to the jet rates was performed to account for the missing higher-order calculations. The fitted scale is called the experimentally optimised scale x_μ^{opt} . The results of the scale-setting methods are shown in Figure 11. Experimentally optimised scales for different fit ranges (indicated by the error bars in y_{cut} -direction) and for several hadronisation models are compared with the theoretical scale evaluations. The fit ranges for x_μ^{opt} are varied between $y_{\text{cut}} = 0.05$ and $y_{\text{cut}} = 0.0005$. Below $y_{\text{cut}} \simeq 0.0005$ the perturbative expansion is expected to become invalid, above $y_{\text{cut}} \simeq 0.05$ the number of events entering R_4 becomes too small to perform the fit. For $y_{\text{cut}} > 0.001$ small values of x_μ are preferred and for y_{cut} near 0.01 the theoretical scale evaluations are of the same magnitude as the experimentally optimised scales.

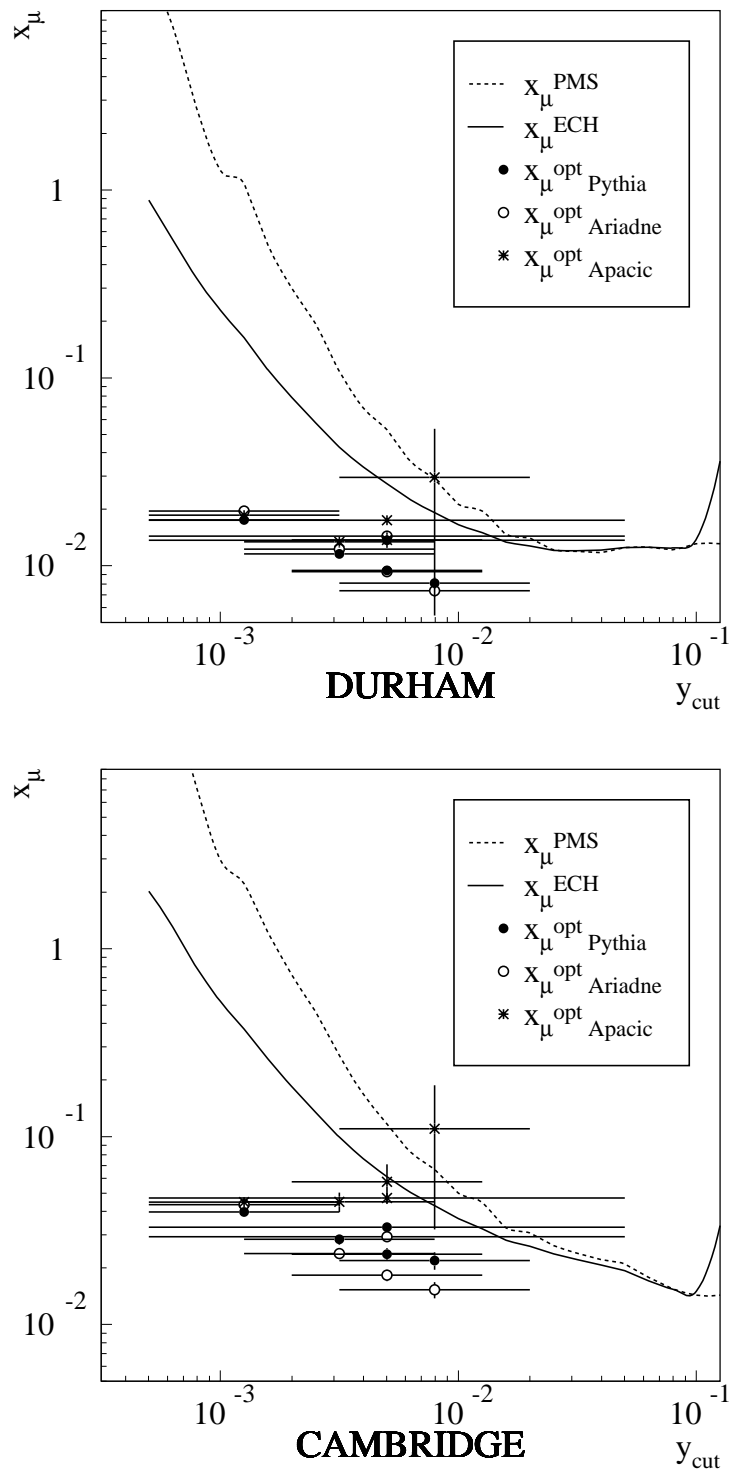


Figure 11: Optimised renormalisation scales: The lines show the y_{cut} dependence for theoretically optimised scales at $E_{cm} = 91$ GeV. The dots give results for experimentally optimised scales. The error bars in the horizontal direction indicate the fit range, the different symbols represent hadronisation corrections applied by different Monte Carlo models.

4.4 Fits to LEP1 data and a precise measurement of $\alpha_s(M_Z^2)$

As discussed above, for each measurement of α_s the renormalisation scale has to be chosen. To determine the experimentally optimised scale a two-parameter fit of Eq. 8 with α_s and x_μ^{opt} as free parameters is performed to the four-jet rate. Table 3 shows the results for x_μ^{opt} .

algorithm	fit range	x_μ^{opt}
DURHAM	0.001 – 0.01	0.015
CAMBRIDGE	0.001 – 0.01	0.042

Table 3: *Experimentally optimised scales.*

Figure 12 shows results of fits using Eq. 8 and the fit ranges given in Table 3 for DURHAM and CAMBRIDGE and for both physical ($x_\mu = 1$) and experimentally optimised scales. While the fit with experimentally optimised scales results in a good agreement with the data over two orders of magnitude in y_{cut} , the fit results with physical scale show a y_{cut} dependence inconsistent with the measurement.

Figure 13 presents results of the α_s fits as a function of y_{cut} for different scale evaluation methods. For fits with physical scale the resulting α_s values show a strong dependence on the choice of y_{cut} . Within the investigated range α_s varies from about 0.1 to 0.13. Theoretically optimised scales (ECH and PMS) improve the situation, but for small values of y_{cut} where the theoretical scales increase, α_s shows again a strong dependence on y_{cut} . Choosing experimentally optimised scales cures the problem. With this choice the α_s results are independent of y_{cut} , and furthermore results for DURHAM and CAMBRIDGE are in good agreement. Experimentally optimised scales are therefore considered as an accurate tool to perform a consistent measurement of the strong coupling from four-jet rates.

The jet rate data, as shown, for instance, in Figure 4, are highly correlated. Therefore a second fit is performed to just one single bin in y_{cut} with α_s as the only free parameter using the fixed scales of Table 3. This final fit is performed at $y_{\text{cut}} = 0.0063$ for both the DURHAM and CAMBRIDGE algorithms. As shown in Figure 13 the fit results are very stable in the vicinity of this y_{cut} value.

The total error on $\alpha_s(M_Z^2)$ is estimated by considering the following experimental and theoretical uncertainties:

- Variations of the track and event cuts given in Table 2: $N_{\text{charged}} \geq (7 \pm 1)$, $E_{\text{tot}} \geq (0.50 \pm 0.05) \cdot E_{\text{cm}}$ and $(25^\circ \pm 5^\circ) \leq \theta_{\text{thrust}} \leq (155^\circ \pm 5^\circ)$.
- In order to account for a remaining dependence on y_{cut} , the working point is varied in the range $0.0016 \leq y_{\text{cut}} \leq 0.01$.
- The difference between fit results in α_s when exchanging the hadronisation model is considered as an estimate of the error due to simulation: This error already includes quark mass effects since the APACIC++ model takes b-quark masses into account.
- To estimate the theoretical error the scale is varied around its optimised value: $0.5 \cdot x_\mu^{\text{opt}} \leq x_\mu \leq 2 \cdot x_\mu^{\text{opt}}$ as in [1], covering the scatter of experimentally optimised scales obtained with different fit ranges and for different hadronisation models, see Figure 11.
- While b-quark mass effects are included in the hadronisation corrections performed with APACIC++ the DEBRECEN generator used to compute the coefficient func-

tion in Equation 8 is available only for the massless case. From recent investigations of b quark mass effects [18] it has been evaluated that these can shift the result by as much as 1.8%. Conservatively a contribution to the uncertainty of this size has been added.

The statistical error, the uncertainties obtained by varying track and event cuts and by varying y_{cut} are combined into the experimental error. Table 4 summarises the contributions to the error on the $\alpha_s(M_Z^2)$ measurement and Table 5 contains the $\alpha_s(M_Z^2)$ results. Within the experimental error the results obtained by using the DURHAM or the CAMBRIDGE algorithm are consistent. The total error on the measurement is 3.0% for DURHAM and 2.6% for CAMBRIDGE. If the scale is varied around its optimised value within the larger range $0.25 \cdot x_\mu^{\text{opt}} \leq x_\mu \leq 4 \cdot x_\mu^{\text{opt}}$ the contribution to the error on $\alpha_s(M_Z^2)$ due to the x_μ variation has to be increased from 0.0014 to 0.0085 for DURHAM and from 0.0007 to 0.0037 for CAMBRIDGE.

contribution to error	DURHAM	CAMBRIDGE
statistical error	0.00045	0.00050
cut variations	0.00041	0.00020
working point variation	0.0011	0.0008
total experimental error	0.0012	0.0010
MC model exchange	0.0023	0.0017
b mass effect	0.0021	0.0021
total had. error	0.0031	0.0027
x_μ variation	0.0014	0.0007
total error on $\alpha_s(M_Z^2)$	0.0036	0.0030

Table 4: *Contribution to the error on $\alpha_s(M_Z^2)$ for DURHAM and CAMBRIDGE.*

observable	$\alpha_s(M_Z^2)$	\pm	exp.	\pm	hadr.	\pm	scale
DURHAM	0.1178	\pm	0.0012	\pm	0.0031	\pm	0.0014
CAMBRIDGE	0.1175	\pm	0.0010	\pm	0.0027	\pm	0.0007

Table 5: *Results in $\alpha_s(M_Z^2)$ for DURHAM and CAMBRIDGE*

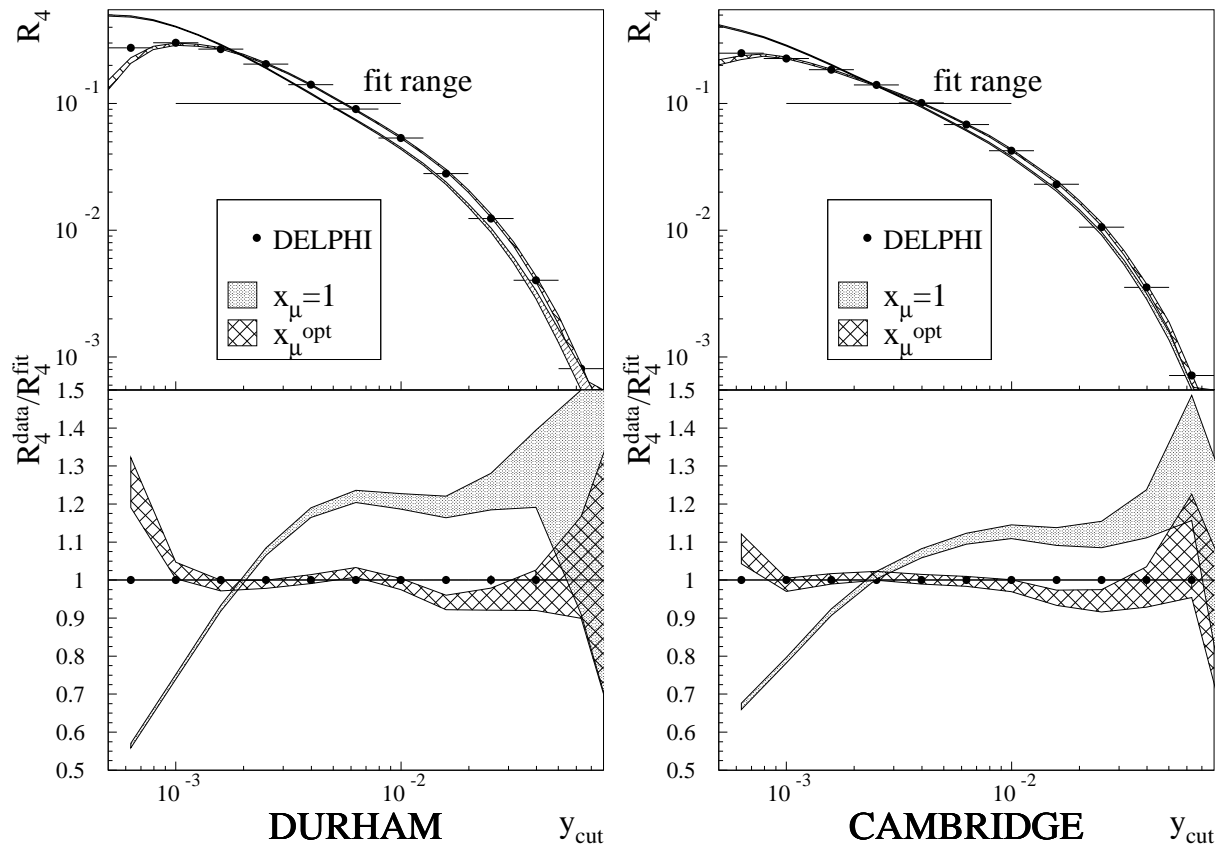


Figure 12: Fits to the four-jet rate R_4 measured at the Z resonance using different scale evaluation methods. Top: the distributions. The hatched curve shows the results for the experimentally optimised scales. Bottom: the ratio $R_4^{\text{data}}/R_4^{\text{fit}}$. The grey bands show fit results with the physical scale ($x_\mu = 1$), the cross-hatched bands for experimentally optimised scales (x_μ^{opt}).

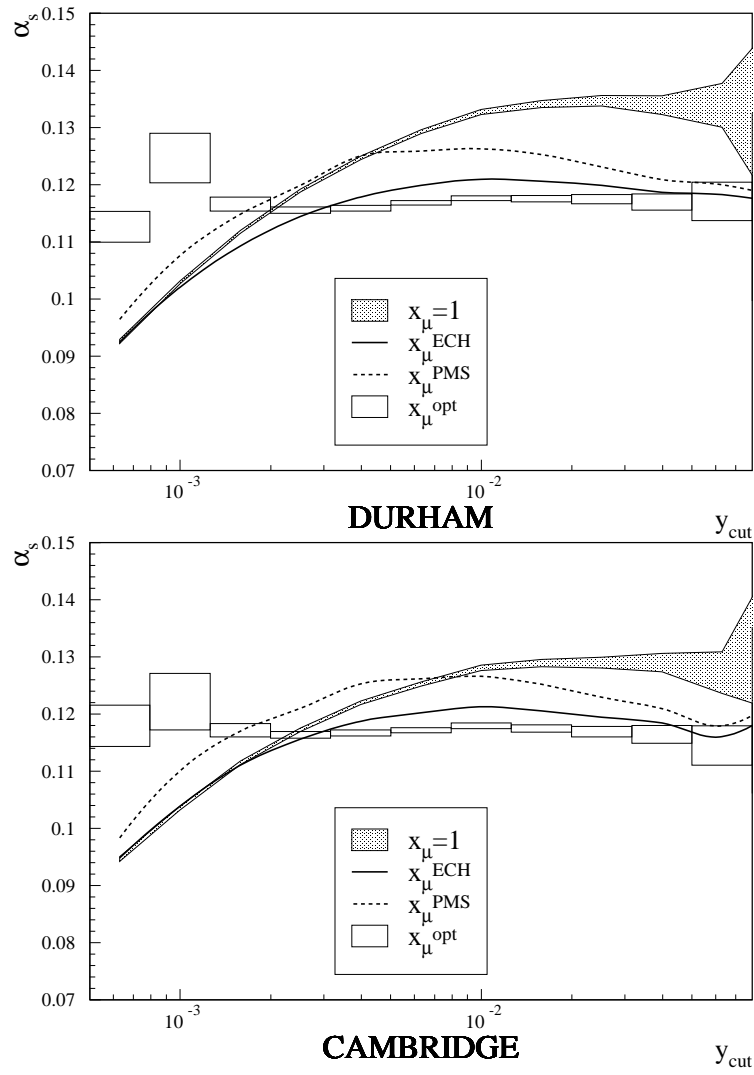


Figure 13: Dependence of α_s on y_{cut} : The grey bands give fit results with physical scale ($x_\mu = 1$), the lines with theoretically optimised scales (ECH, PMS) and the rectangles with experimentally optimised scales (x_μ^{opt}).

4.5 Measurement of the running of α_s

To investigate the energy dependence of the strong coupling constant α_s , the fits to the four-jet rates (with optimised scales, as determined in Sec. 4.3) are repeated at all centre-of-mass energies listed in Table 1. In order to account for the lower statistics of the LEP2 data, the working points are shifted to smaller values of y_{cut} which, however, are still in the range of stable α_s results: DURHAM $y_{\text{cut}} = 0.0040$, CAMBRIDGE $y_{\text{cut}} = 0.0025$.

The determination of α_s at different energies allows the predicted scale dependence of the coupling due to higher order effects to be tested. Starting from the renormalisation group equation:

$$E_{\text{cm}}^2 \frac{d\alpha_s}{dE_{\text{cm}}^2} = \beta(\alpha_s) = -\alpha_s^2(b_0 + b_1\alpha_s + \dots), \quad (12)$$

the logarithmic energy slope is obtained:

$$\frac{d\alpha_s^{-1}}{d \log(E_{\text{cm}})} = -\frac{2}{\alpha_s^2} \beta(\alpha_s) = 2b_0 \left(1 + \frac{b_1}{b_0} \alpha_s + \dots\right) = 2b_0 \left(1 + \frac{b_1}{b_0^2 \log(E_{\text{cm}}^2/\Lambda^2)} + \dots\right), \quad (13)$$

with $b_0 = (33 - 2n_f)/12\pi$, $b_1 = (153 - 19n_f)/24\pi^2$. In leading order the logarithmic derivative (Eq. 13) is independent of α_s and E_{cm} and twice the coefficient b_0 of the β function ($2b_0 = 1.22$ for $n_f = 5$). Evaluating the equation in second order results in a small dependence of the derivative on α_s . Thus Λ_{QCD} and an appropriate energy scale have to be chosen in order to calculate a single value of the logarithmic derivative which can be compared with the experimental result. Using $E_{\text{cm}} = 150 \pm 60$ GeV (the average energy of our measurements), $\Lambda = 230$ MeV (corresponding to $\alpha_s(M_Z) = 0.118$), and $n_f = 5$ one obtains $d\alpha_s^{-1}/d \log E_{\text{cm}} = 1.27 \pm 0.10$.

The experimental value of $d\alpha_s^{-1}/d \log E_{\text{cm}}$ as obtained from fitting the function $1/(a \log E_{\text{cm}} + b)$ to the measured α_s values is in good agreement with the QCD expectation (Table 6 and Figure 14).

The following contributions to the systematic error on the logarithmic derivative are considered:

- Since the acceptance corrections C_{acc} (Eq. 2) are correlated between all energies, a possible systematic error would have only a reduced influence on the logarithmic energy slope of α_s . Still the acceptance correction is energy-dependent. To evaluate the corresponding systematic error, the difference between the correction factor C at the Z pole and at LEP2 energies is added to C at the three energies near the Z resonance at 89, 91, and 93 GeV and the fit is repeated. The full difference in the slopes found with or without this change is considered as the contribution to the systematic error of the logarithmic slope due to the acceptance correction.
- At LEP2 energies the cut in the reconstructed centre-of-mass energy is changed from $\sqrt{s'_{\text{rec}}} \geq 0.9 \cdot E_{\text{cm}}$ to $\sqrt{s'_{\text{rec}}} \geq 0.8 \cdot E_{\text{cm}}$ and the fit is repeated. The difference in the logarithmic slopes is taken as the contribution to the systematic error.
- The treatment of 4f background is an important source of systematic uncertainties.
 - The 4f simulation is performed by using alternatively PYTHIA or EXCALIBUR, the full difference being included as the systematic error.
 - For the subtraction of 4f background the cross-section is varied by its total error on $\pm 1.5\%$.
 - The cut in the discriminating variable is varied: $D^2 > (900 \pm 100) \text{ GeV}^2$.
- The renormalisation scale is varied at all energies: $1/2 \cdot x_\mu^{\text{opt}} \leq x_\mu \leq 2 \cdot x_\mu^{\text{opt}}$.

Effects due to track and event selections are regarded as fully correlated between the energies and thus neglected. Table 6 contains the results of the $d\alpha_s^{-1}/d\log E_{\text{cm}}$ measurements for the DURHAM and CAMBRIDGE algorithms and the corresponding statistical and systematical errors.

Observable	$d\alpha_s^{-1}/d\log E_{\text{cm}}$
DURHAM	$1.21 \pm 0.26 \pm 0.20$
CAMBRIDGE	$1.14 \pm 0.25 \pm 0.26$
QCD expectation	1.27

Table 6: Results of the $d\alpha_s^{-1}/d\log E_{\text{cm}}$ measurements for the DURHAM and CAMBRIDGE algorithms. The theoretical expectation is calculated in second order.

5 Summary

Hadronic jet rates in electron-positron annihilation have been measured by DELPHI at centre-of-mass energies between 89.4 and 209 GeV. The data agree with the expectation from QCD-based event generators. No indication of a significant excess of multijet events at high energies is found.

The strong coupling constant has been determined from the four-jet rate in $\mathcal{O}(\alpha_s^3)$. A variety of methods to solve the renormalisation scale problem has been investigated. A consistent measurement of α_s can be performed by using experimentally optimised scales. The results obtained with two different jet-clustering algorithms agree. The final result quoted is obtained by applying the CAMBRIDGE algorithm, since this algorithm has small third-order contributions, and shows a smaller dependence on the renormalisation scale:

$$\alpha_s(M_Z^2) = 0.1175 \pm 0.0030 \text{ (tot)}. \quad (14)$$

The result in $\mathcal{O}(\alpha_s^3)$ is statistically uncorrelated and in good agreement with previous DELPHI measurements [1] and also with the world average value [28]. The α_s result is also in good agreement with recent α_s measurements of the OPAL [29] and ALEPH [30] collaborations based on four-jet rates measured at the Z resonance using $\mathcal{O}(\alpha_s^3)$ calculations combined with the resummation of large logarithms. The scale-setting methods obtained in [1] are confirmed.

The comparison of α_s as measured at the Z and at higher energies confirms that the energy dependence of the strong coupling is consistent with QCD expectation. Results from DURHAM and CAMBRIDGE are consistent. The logarithmic energy slope, again obtained from CAMBRIDGE and again statistically uncorrelated to the result of the $\mathcal{O}(\alpha_s^2)$ analysis presented in [31], is measured to be

$$\frac{d\alpha_s^{-1}}{d\log E_{\text{cm}}} = 1.14 \pm 0.36 \text{ (tot)}, \quad (15)$$

while the QCD prediction for this quantity is 1.27. The measurement is in good agreement with previous measurements in $\mathcal{O}(\alpha_s^2)$ [2, 31].

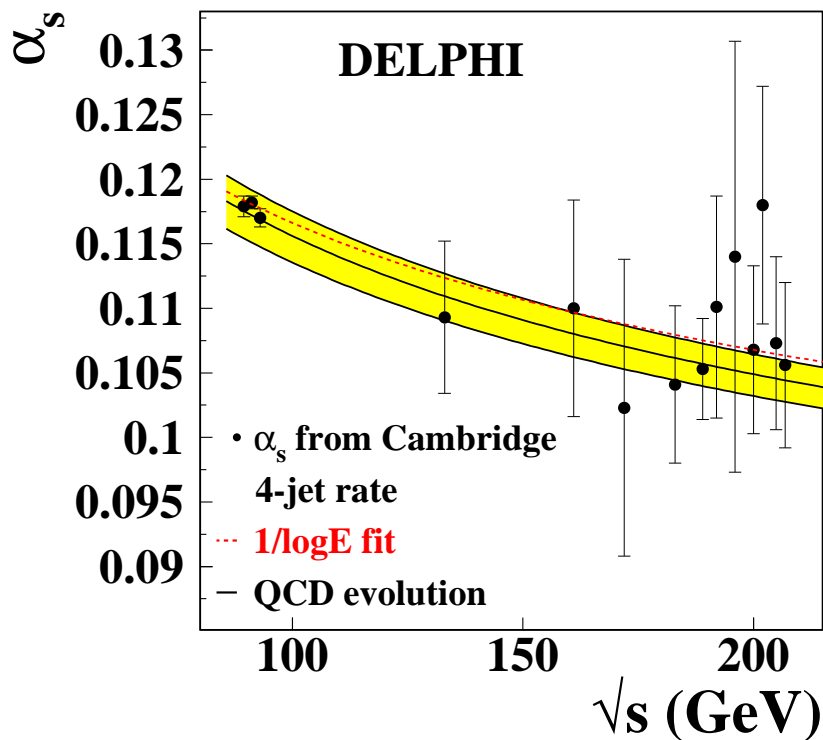
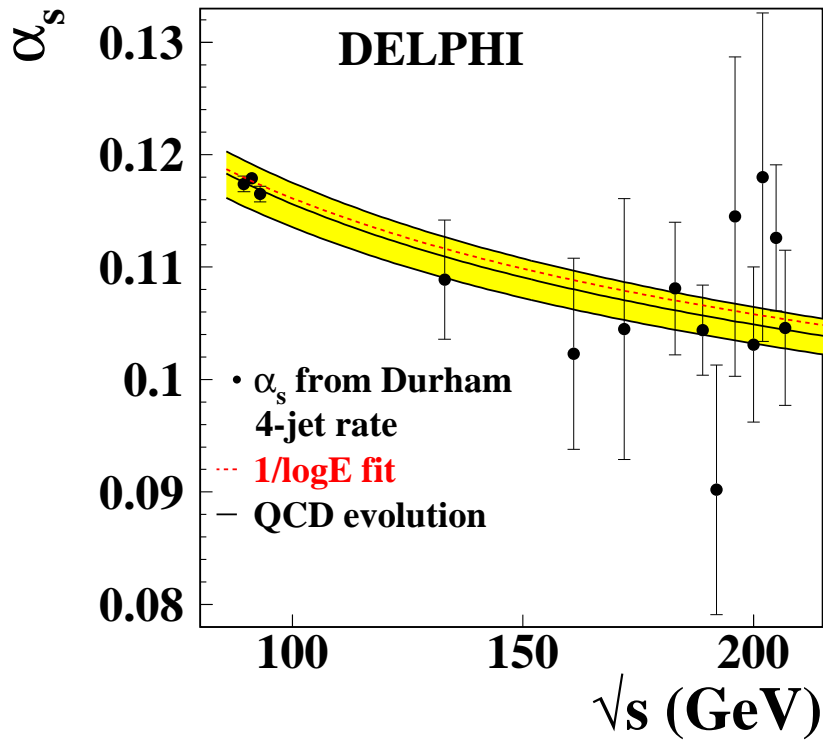


Figure 14: Energy dependence of α_s as obtained from jet rates with experimentally optimised scales. The errors shown are statistical only. The band shows the QCD expectation when extrapolating the world average [28] to other energies. The dashed lines show the result of the $1/\log\sqrt{s}$ fits.

Acknowledgements

We are greatly indebted to our technical collaborators, to the members of the CERN-SL Division for the excellent performance of the LEP collider, and to the funding agencies for their support in building and operating the DELPHI detector.

We acknowledge in particular the support of

Austrian Federal Ministry of Science and Traffics, GZ 616.364/2-III/2a/98,

FNRS-FWO, Belgium,

FINEP, CNPq, CAPES, FUJB and FAPERJ, Brazil,

Czech Ministry of Industry and Trade, GA CR 202/96/0450 and GA AVCR A1010521,

Danish Natural Research Council,

Commission of the European Communities (DG XII),

Direction des Sciences de la Matière, CEA, France,

Bundesministerium für Bildung und Forschung, Germany,

General Secretariat for Research and Technology, Greece,

National Science Foundation (NWO) and Foundation for Research on Matter (FOM),

The Netherlands,

Norwegian Research Council,

State Committee for Scientific Research, Poland, 2P03B06015, 2P03B03311 and SPUB/P03/178/98,

JNICT-Junta Nacional de Investigação Científica e Tecnológica, Portugal,

Vedecka grantova agentura MS SR, Slovakia, Nr. 95/5195/134,

Ministry of Science and Technology of the Republic of Slovenia,

CICYT, Spain, AEN96-1661 and AEN96-1681,

The Swedish Natural Science Research Council,

Particle Physics and Astronomy Research Council, UK,

Department of Energy, USA, DE-FG02-94ER40817.

References

- [1] DELPHI Coll., P. Abreu et al., *Eur. Phys. J.* **C14** (2000) 557.
- [2] DELPHI Coll., P. Abreu et al., *Phys. Lett.* **B456** (1999) 322.
- [3] D. Bardin et al., *Comput. Phys. Commun.* **133** (2001) 229.
- [4] DELPHI Coll., P. A. Aarnio et al., *Nucl. Instrum. Meth.* **A303** (1991) 233.
- [5] DELPHI Coll., P. Abreu et al., *Nucl. Instrum. Meth.* **A378** (1996) 57.
- [6] P. Abreu et al., *Nucl. Instrum. Meth.* **A427** (1999) 487.
- [7] K. H. Becks et al., *Nucl. Instrum. Meth.* **A426** (1999) 599.
- [8] F. A. Berends, R. Pittau and R. Kleiss, *Comput. Phys. Commun.* **85** (1995) 437.
- [9] F. Berends, R. Pittau and R. Kleiss, *Nucl. Phys.* **B426** (1994) 344.
- [10] S. Jadach et al., *CERN Report* 2000-009 (2000) 31.
- [11] V. S. Fadin et al., *Phys. Lett.* **B363** (1995) 112.
- [12] T. Sjostrand, *PYTHIA 5.7 and JETSET 7.4: Physics and Manual*, CERN-TH-7112-93.
- [13] T. Sjostrand, *Comput. Phys. Commun.* **39** (1986) 347.
- [14] DELPHI Coll., P. Abreu et al., *Z. Phys.* **C73** (1996) 11.
- [15] JADE Coll., W. Bartel et al., *Z. Phys.* **C 33** (1986) 23.
- [16] Y. Dokshitzer et al., *Phys. Lett.* **B 269** (1991) 432.
- [17] Y. Dokshitzer et al., *JHEP* 9708 (1997) 001

- [18] A. Ballestrero et al., Report of the QCD working group CERN 2000-009 (2000) 137.
- [19] L. Lonnblad, *Comput. Phys. Commun.* **71** (1992) 15.
- [20] G. Marchesini et al., *Comp. Phys. Comm.* **67** (1992) 465.
- [21] R. Kuhn et al., *Comput. Phys. Commun.* **134** (2001) 223.
- [22] F. Krauss, R. Kuhn and G. Soff, *Acta Phys. Polon.* **B30** (1999) 3875.
- [23] F. Krauss, R. Kuhn and G. Soff, *J. Phys.* **G26** (2000) L11–L15.
- [24] Z. Nagy and Z. Trocsanyi, *Phys. Rev.* **D59** (1999) 014020; erratum ibd. **D62** (2000) 099902.
- [25] Z. Nagy and Z. Trocsanyi, *Phys. Rev. Lett.* **79** (1997) 3604.
- [26] G. Grunberg, *Phys. Rev.* **D29** (1984) 2315.
- [27] P. M. Stevenson, *Phys. Rev.* **D23** (1981) 2916.
- [28] Particle Data Group, K. Hagiwara et al., *Phys. Rev.* **D66** (2002) 010001.
- [29] OPAL Coll., G. Abbiendi et al., *Eur. Phys. J.* **C20** (2001) 601.
- [30] ALEPH Coll., A. Heister et al., *Eur. Phys. J.* **C27** (2003) 1.
- [31] DELPHI Coll., J. Abdallah et al., *Eur. Phys. J.* **C37** (2004) 1.